

Supporting information

Effect of nanosecond-pulsed plasma on the structural modification of biomolecules

Ji Hoon Park,¹ Naresh Kumar,¹ Han Sup Uhm,¹ Weontae Lee,² Eun Ha Choi^{1*} and Pankaj Attri,^{1*}

¹*Plasma Bioscience Research Center / Department of Electrical and Biological Physics, Kwangwoon University, Seoul, Korea 139-701.*

²*Department of Biochemistry, College of Life Science & Biotechnology, Yonsei University, Seoul, 120-749, Korea*

Nanosecond-Pulsed Plasma (NPP) in liquid using a Marx Generator. We used a Marx generator, which is the most simple and widely used high-voltage pulse generation device, to generate nanosecond-pulsed plasma in liquid.¹ The basic operating principle of the device is to charge a set of capacitors in parallel and then discharge them in series. The Marx generator used in this study consisted of 5 stages. Each capacitor (of a total of five capacitors) had a capacitance of 0.5 μF and was connected in parallel to a 60 k Ω resistor. Every spark switch is made from brass and is located on a Lucite tube, which has a diameter of 100 mm and a thickness of 4 mm. Every spark switch is connected to the circuit through the Lucite tube by using a screw, and switching is induced by generating the first spark gap after charging the capacitors, as shown in Figure S1a.

We used two types of electrodes, point electrodes with a diameter of 1 mm and plane-plane electrodes with a 8-mm diameter. Both types of electrodes were made of stainless steel, which has high stability even when elevated temperatures are achieved in the cylindrical tube. For the experiment, the distance of the electrode located within the cylindrical tube was fixed at 8 mm. The cylindrical tube had a length of 320 mm, an external diameter of 50 mm, and an inner diameter of 10 mm. The breakdown voltage and current were measured for each type of electrode by using a Tektronix 1000:1 probe (P6015A) and a Pearson Current Monitor with a Rogowski coil (Model No. 411; output volts per ampere, 0.1). The breakdown voltage and current were measured to be 14 kV and 0.6 kA for the point-point electrode and 12 kV and 0.7 kA for the plane-plane electrodes. The product of the breakdown voltage and the current were integrated with respect to time during the breakdown times to reveal a breakdown energy of 0.103 J for the point electrodes and 0.106 J for the plane electrodes. Moreover, the breakdown time for the point and plane electrodes were measured

to be 500 ns and 600 ns, respectively, as shown in Table S1. Single-shot images are visible using a pinhole camera (the pinhole camera has a 32-mm focal length and a 0.25-mm pinhole diameter), as shown in FigureS1b.

For better understanding the discharge parameters, we have examined the electron density and electron temperature. Plasma electron density was obtained using the Stark broadening of the H_β line (486.1 nm) from the line full width at half maximum (FWHM) using below as mention in reported work.²

$$FWHM \Delta\lambda_{FWHM} = 4.800 \text{ nm} \times \left(\frac{N_e}{10^{23} \text{ m}^{-3}} \right)^{0.68116}$$

Assuming partial local thermal equilibrium, the electron density can be derived. The electron density was measure to be $1.33 \times 10^{21} \text{ m}^{-3}$ for the point-point electrodes and $1.48 \times 10^{21} \text{ m}^{-3}$ for the plane-plane electrodes. Electron temperature was measure using the Boltzmann plot and SPECAIR software. Using the Boltzmann plot we observed the electron temperature of $\approx 0.7\text{eV}$ for plane to plane electrode and $\approx 0.8 \text{ eV}$ for the point to point electrode, while using SPECAIR software we obtained the electron temperature $\approx 0.85\text{eV}$ for plane to plane electrode and $\approx 0.91\text{eV}$ for the point to point electrode, which is quite near to the our experimental data.

Hb and Mb protein oxidation.^{3,4} Cold trichloroacetic acid was used to precipitate Hb and Mb to a final concentration of 10% (v/v). The samples were centrifuged at 11,000 g for 3 min after a 10 min incubation period at 4 °C, followed by resuspension of the Hb and Mb pellets in 0.5 ml of 10 mM 2,4-dinitrophenylhydrazine (DNPH) / 2 M HCl. The samples were placed in a sample holder, vortexed continuously at room temperature for 1 h, and then precipitated with 0.5 mL of 20% TCA followed by centrifugation at 11,000 g for 3 min. Free DNPH reagent was removed by washing the pellet with 1 ml of ethanol-ethyl acetate [1:1 (v/v)] and then allowing to stand for 10 min. The sample was then centrifuged for 5 min at 11,000 g, and the supernatant was discarded. The washing procedure was repeated twice.

After completing the above steps, the resulting Hb and Mb pellets were resuspended in 1.0 mL of 6 M guanidine with 2 mM potassium phosphate buffer (pH 2.3, adjusted with trifluoroacetic acid), and the samples were incubated at 37 °C for 15–30 min to aid the Hb and Mb dissolution. The samples that had difficulty going into solution were briefly sonicated and

incubated at an increased temperature of upto 70 °C. The insoluble materials remaining in the suspension were removed by centrifuging all of the samples. The DNPH concentration was determined at its maximum wavelength of 360 nm, and the oxidation levels of the proteins were quantified by using a molar absorption coefficient of 22, 000 M⁻¹ cm⁻¹. The protein oxidation content was expressed as a percentage compared to control.

Reference

1. P. Attri, J. H. Park, J. Gaur, N. Kumar, D. H. Park, S. N. Jeon, B. S. Park, S. Chand, H. S. Uhm and E. H. Choi, *Phys. Chem. Chem. Phys.*, 2014, **16**, 18375–18382.
2. P. Bruggeman, D. Schram, M. Á González, R. Rego, M. G. Kong and C. Leys, *Plasma Sources Sci. Technol.*, 2009, **18** 025017
3. P. Attri, N. Kumar, J. H. Park, D. K. Yadav, S. Choi, H. S. Uhm, I. T. Kim, E. H. Choi and W. Lee, *Sci. Rep.*, 2015, **5**, 8221.
4. L. J. Yan, and M. J. Forster, *J. Chromatogr. B Analyt. Technol. Biomed. Life Sci.* 2011, **879**, 1308–1315.

Fig. S1. (a) Schematic diagram of nanosecond-pulsed plasma (NPP) using Max Generator setup; (b) The pinhole camera image of the spark produces in the water. The pinhole camera has the focal length of 32 mm and pinhole diameter of 0.25 mm.

Fig. S2. (a) The emission spectrum between 200 and 1100 nm from NPP in distilled water using both electrodes; (b) Raman spectra of the H₂O, H₂O treated with point and plane electrode and H₂O₂ (30%) after binding with titanly ion after 4th NPP exposure.

Fig. S3. H₂O₂, NO, pH and temperature in water exposed to point and plane electrodes for different number of discharges.

Fig. S4. Near-UV CD spectra analysis of (a) Hb point; (b) Mb point; (c) Hb plane and (d) Mb plane, where proteins without treatment (black), 1st discharge of point and plane electrodes (red), 2nd discharge of point and plane electrodes (blue), 3rd discharge of point and plane electrodes (green) and 4th discharge of point and plane electrodes (magenta). The data points are average values of at least six determinations, the error bars indicating ± mean deviation.

Fig. S5. Gel electrophoresis after each discharge using point and plane electrodes (a) Hb and (b) Mb

Fig. S6. MALDI TOF mass spectra of (a) Mb (control); (b) Mb after the 4th discharge using

point electrodes and (c) Mb after the 4th discharge using plane electrodes.

Fig. S7. ¹H NMR data for Mb and Hb before and after the 4th discharge with both electrodes

Fig. S8. Liquid Chromatograph /Capillary Electrophoresis- Mass Spectrometer (LC/CE-MS) based qualitative bioanalysis of Asparagine control.

Fig. S9. Liquid Chromatograph /Capillary Electrophoresis- Mass Spectrometer (LC/CE-MS) based qualitative bioanalysis of Asparagine + point electrode.

Fig. S10. Liquid Chromatograph /Capillary Electrophoresis- Mass Spectrometer (LC/CE-MS) based qualitative bioanalysis of Asparagine + plane electrode.

Fig. S11. Liquid Chromatograph /Capillary Electrophoresis- Mass Spectrometer (LC/CE-MS) based qualitative bioanalysis of Glutamic acid control.

Fig. S12. Liquid Chromatograph /Capillary Electrophoresis- Mass Spectrometer (LC/CE-MS) based qualitative bioanalysis of Glutamic acid + point electrode.

Fig. S13. Liquid Chromatograph /Capillary Electrophoresis- Mass Spectrometer (LC/CE-MS) based qualitative bioanalysis of Glutamic acid + plane electrode.

Fig. S14. Liquid Chromatograph /Capillary Electrophoresis- Mass Spectrometer (LC/CE-MS) based qualitative bioanalysis of Glycine control.

Fig. S15. Liquid Chromatograph /Capillary Electrophoresis- Mass Spectrometer (LC/CE-MS) based qualitative bioanalysis of Glycine + point electrode.

Fig. S16. Liquid Chromatograph /Capillary Electrophoresis- Mass Spectrometer (LC/CE-MS) based qualitative bioanalysis of Glycine + plane electrode

Fig. S17. Liquid Chromatograph /Capillary Electrophoresis- Mass Spectrometer (LC/CE-MS) based qualitative bioanalysis of Lysine control

Fig. S18. Liquid Chromatograph /Capillary Electrophoresis- Mass Spectrometer (LC/CE-MS) based qualitative bioanalysis of Lysine + point electrode.

Fig. S19. Liquid Chromatograph /Capillary Electrophoresis- Mass Spectrometer (LC/CE-MS) based qualitative bioanalysis of Lysine + plane electrode.

Fig. S20. Liquid Chromatograph /Capillary Electrophoresis- Mass Spectrometer (LC/CE-MS) based qualitative bioanalysis of Proline control.

Fig. S21. Liquid Chromatograph /Capillary Electrophoresis- Mass Spectrometer (LC/CE-MS) based qualitative bioanalysis of Proline + point electrode.

Fig. S22. Liquid Chromatograph /Capillary Electrophoresis- Mass Spectrometer (LC/CE-MS) based qualitative bioanalysis of Proline + plane electrode.

Fig. S23. Liquid Chromatograph /Capillary Electrophoresis- Mass Spectrometer (LC/CE-MS) based qualitative bioanalysis of Threonine control.

Fig. S24. Liquid Chromatograph /Capillary Electrophoresis- Mass Spectrometer (LC/CE-MS) based qualitative bioanalysis of Threonine + point electrode.

Fig. S25. Liquid Chromatograph /Capillary Electrophoresis- Mass Spectrometer (LC/CE-MS) based qualitative bioanalysis of Threonine + plane electrode.

Table S1. Physical parameters of the NPP discharges in both electrodes

Electrodes	Peak Voltage	Peak Current	Breakdown Voltage	Breakdown Current	Breakdown Time	Breakdown Energy
Point-point	26 kV	3.5 kA	14 kV	0.6 kA	500 ns	0.103 J
Plane-plane	24 kV	3.6 kA	12 kV	0.7 kA	600 ns	0.106 J

Table S2. Secondary structure, composition of Hb and Mb, determined from Far UV CD spectra after treatment with different electrodes at 25 °C determined by K2D3.

Number of Discharge	α -helix (%)	β -sheet (%)
Hb	67.88	9.19
Hb + 1 st discharge point	67.61	9.23
Hb + 2 nd discharge point	67.56	9.33
Hb + 3 rd discharge point	67.49	9.56
Hb + 4 th discharge point	67.01	9.87
Mb	84.39	0.84
Mb + 1 st discharge point	84.16	0.89
Mb + 2 nd discharge point	83.07	0.91
Mb + 3 rd discharge point	81.1	0.94
Mb + 4 th discharge point	79.05	1.12
Hb + 1 st discharge plane	67.70	9.00
Hb + 2 nd discharge plane	67.60	9.32
Hb + 3 rd discharge plane	67.11	9.34
Hb + 4 th discharge plane	66.55	9.36
Mb + 1 st discharge plane	84.39	0.84
Mb + 2 nd discharge plane	84.06	0.86
Mb + 3 rd discharge plane	82.59	0.89
Mb + 4 th discharge plane	77.66	0.89

Table S3. Transition temperature (T_m) determined by CD analysis

Sample	$T_m/^{\circ}\text{C}$
Mb	83.16 ± 0.11
Mb + 1 st discharge plane	81.26 ± 0.33
Mb + 2 nd discharge plane	80.86 ± 0.12
Mb + 3 rd discharge plane	79.26 ± 0.13
Mb + 4 th discharge plane	78.12 ± 0.56
Mb + 1 st discharge point	82.49 ± 0.67
Mb + 2 nd discharge point	81.30 ± 0.88
Mb + 3 rd discharge point	80.67 ± 0.99
Mb + 4 th discharge point	80.30 ± 1.2
Hb	63.69 ± 0.13
Hb + 1 st discharge plane	63.16 ± 0.69
Hb + 2 nd discharge plane	58.76 ± 0.73
Hb + 3 rd discharge plane	56.67 ± 0.40
Hb + 4 th discharge plane	55.34 ± 0.33
Hb + 1 st discharge	63.17 ± 0.68

point	
Hb + 2 nd discharge point	62.19 ± 0.38
Hb + 3 rd discharge point	60.93 ± 0.16
Hb + 4 th discharge point	58.58 ± 0.36

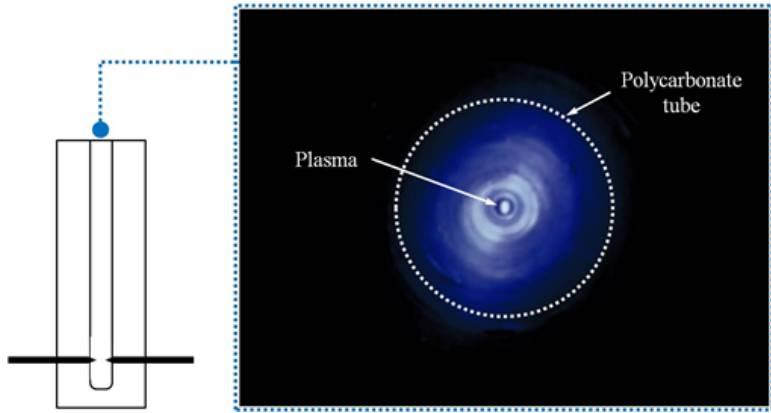
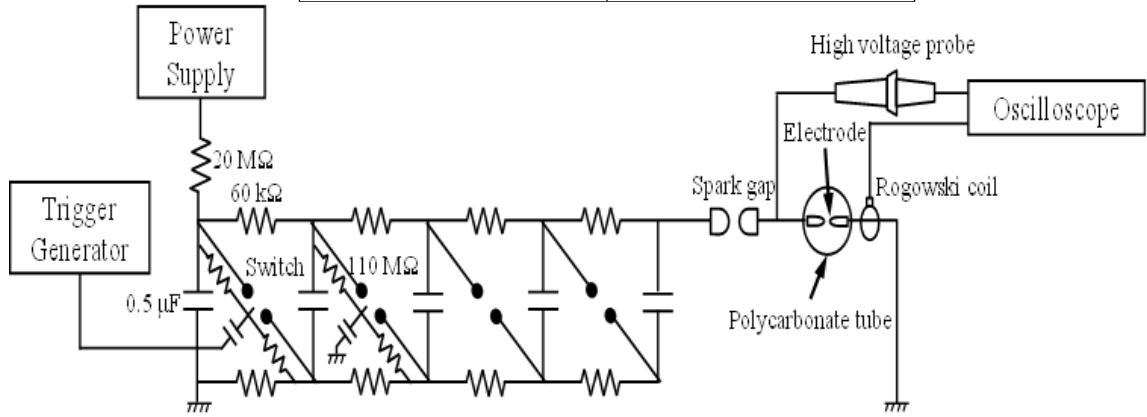


Fig. S1

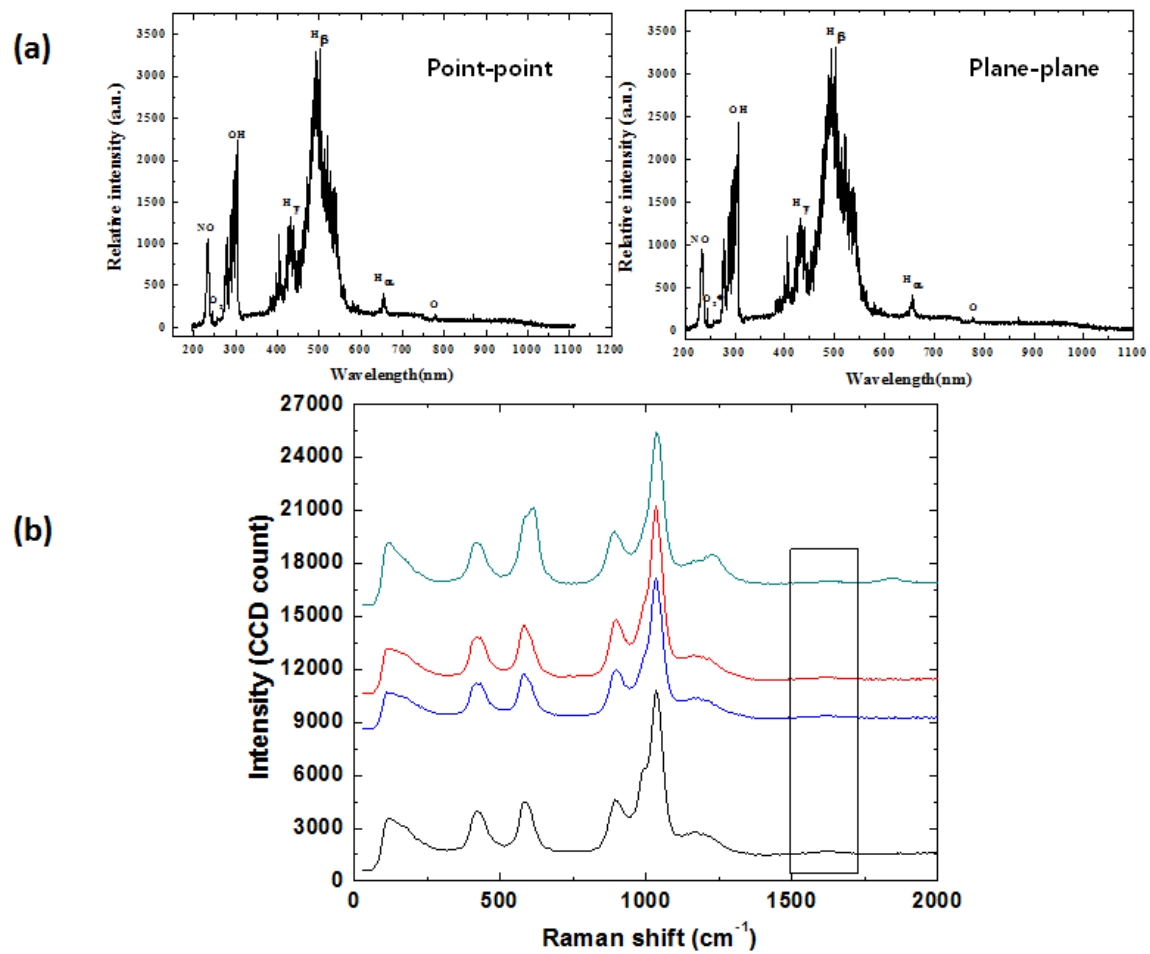


Fig. S2

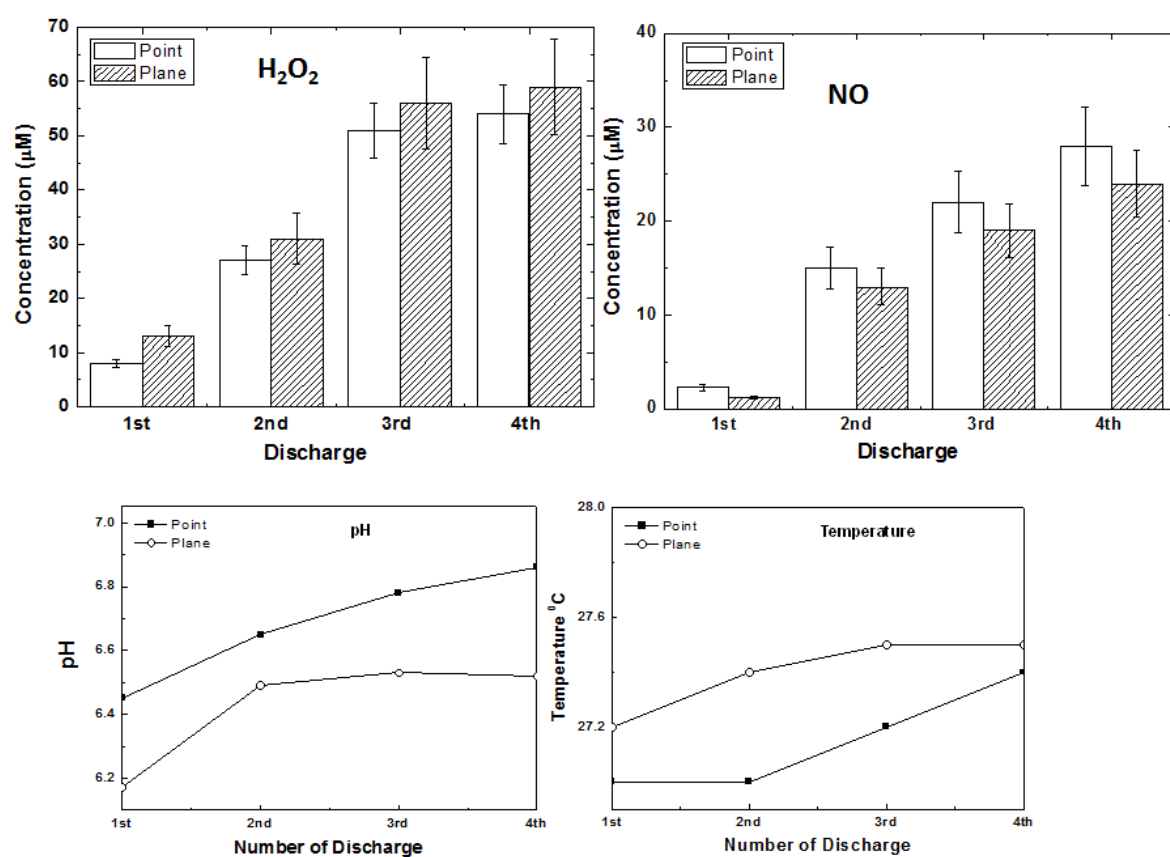


Fig. S3

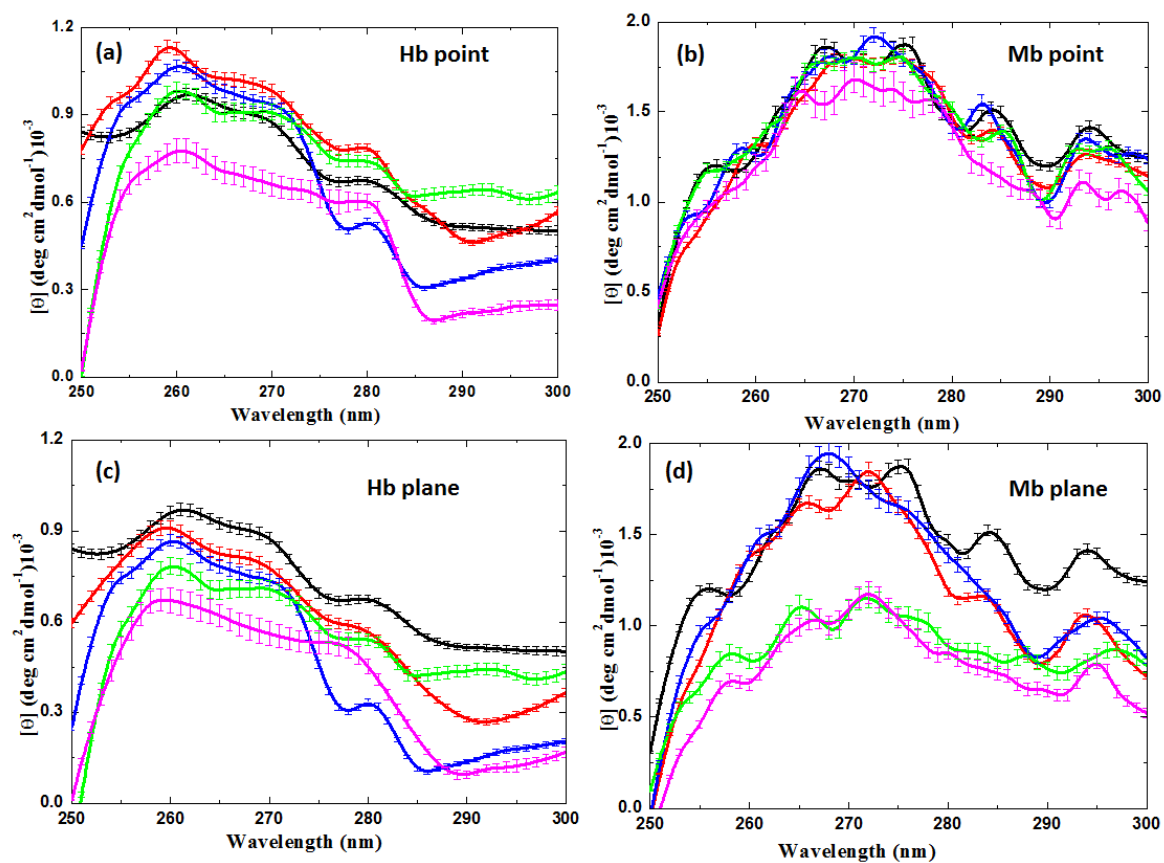


Fig. S4

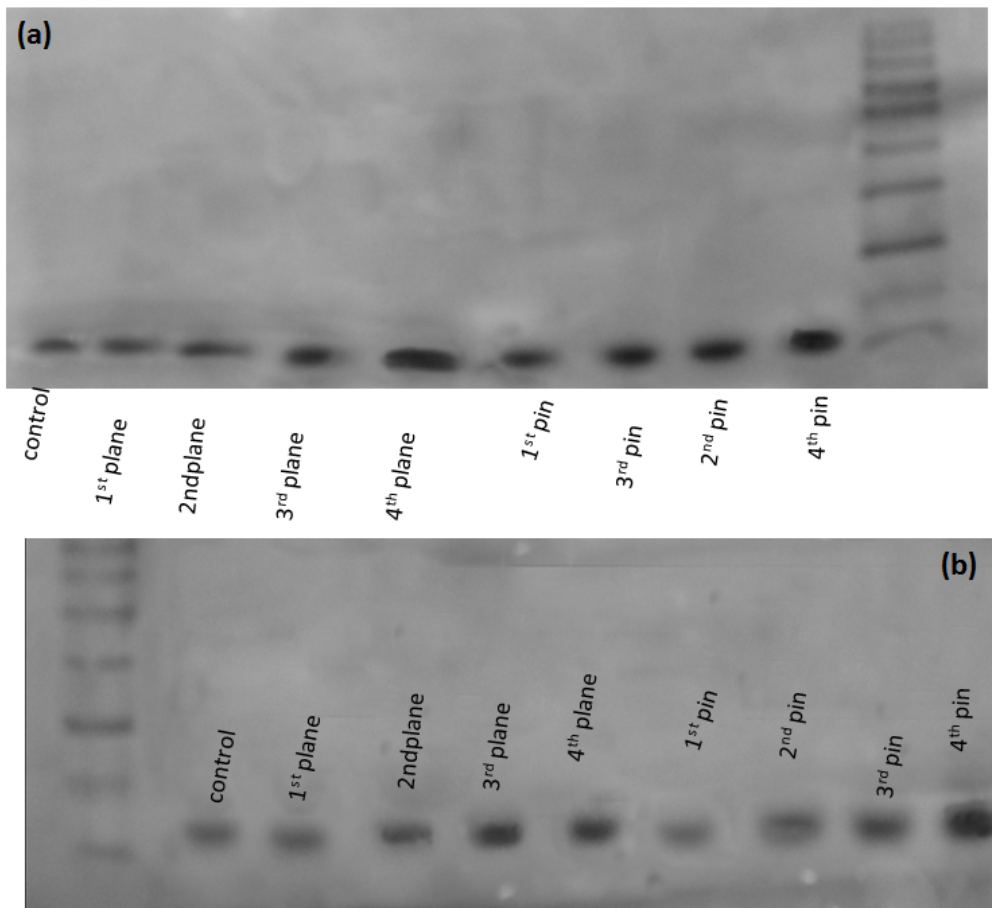


Fig. S5

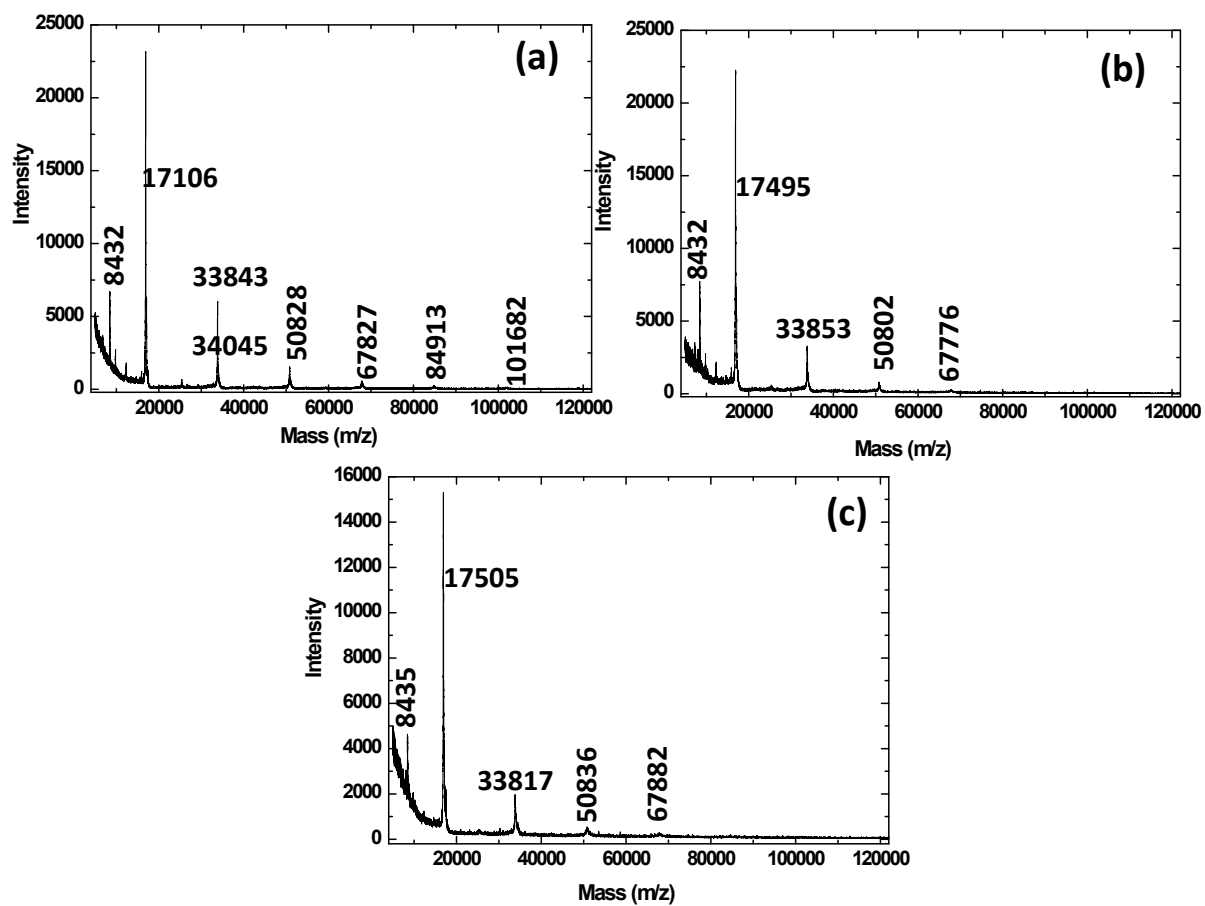
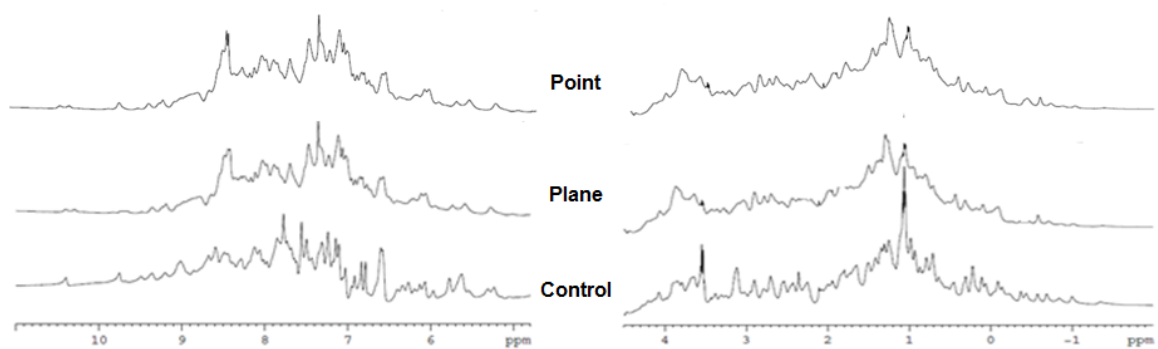


Fig. S6

Mb



Hb

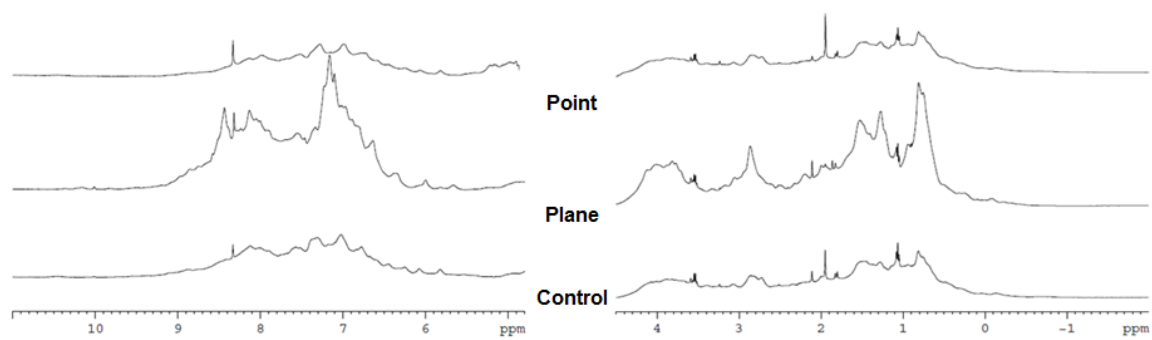


Fig. S7

Asparagine Control

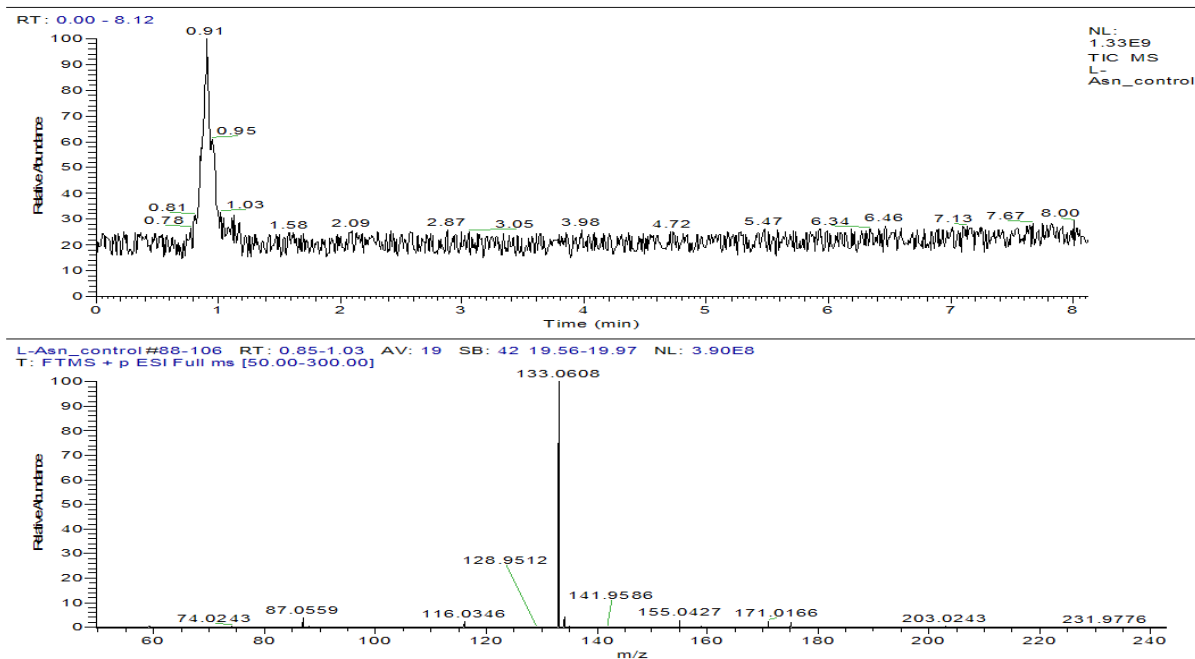


Fig. S8.

Asparagine Point

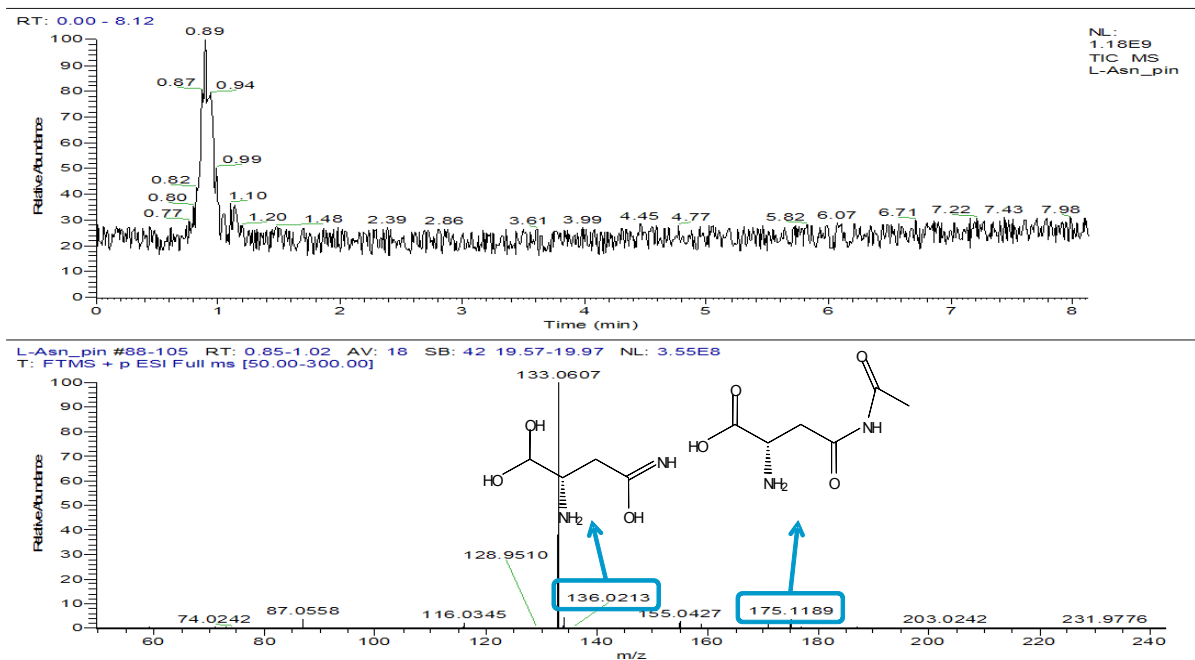


Fig. S9.

Asparagine Plane

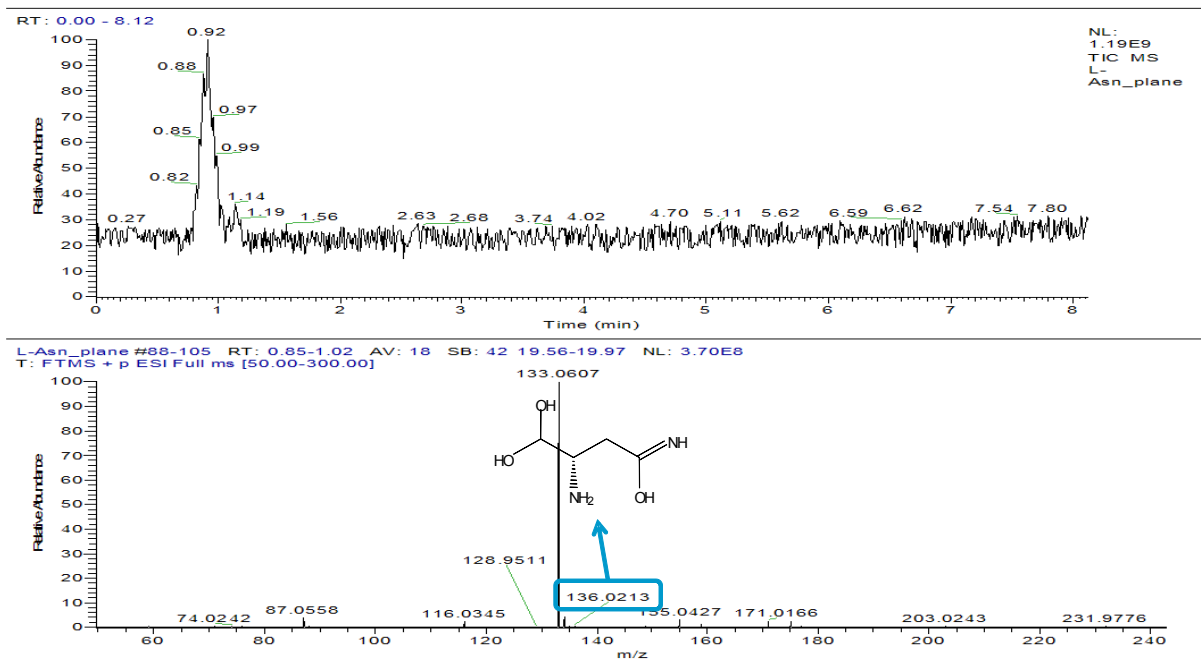


Fig. S10.

Glutamic acid Control

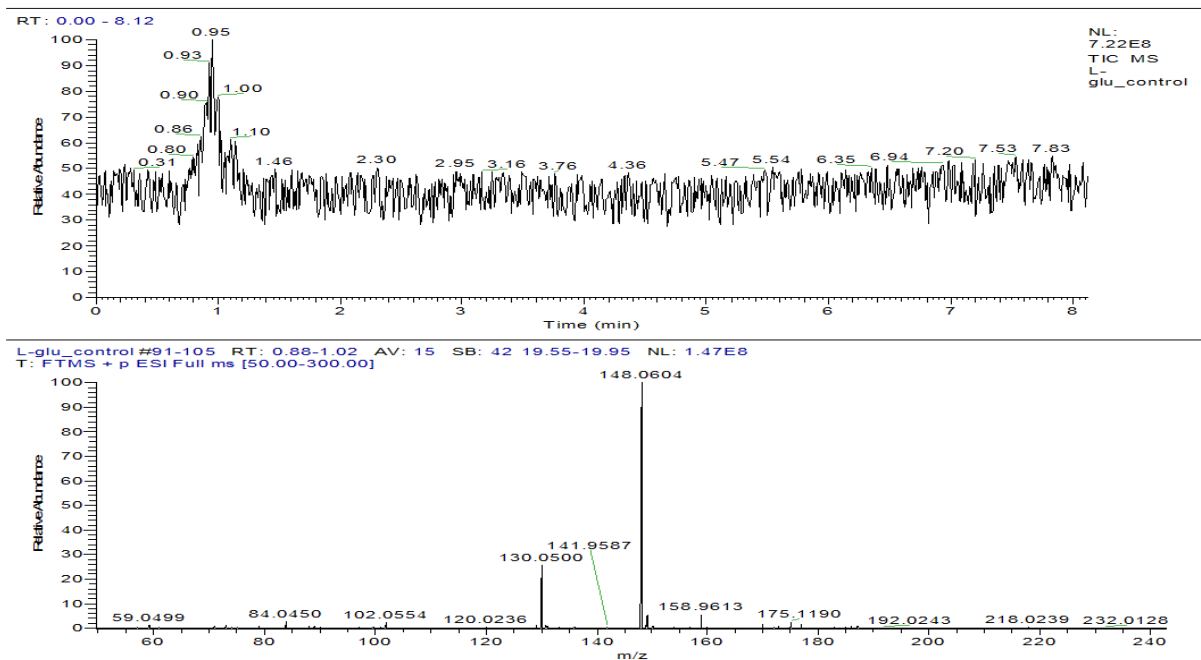


Fig. S11.

Fig. S12.

Fig. S13.

Glycine Control

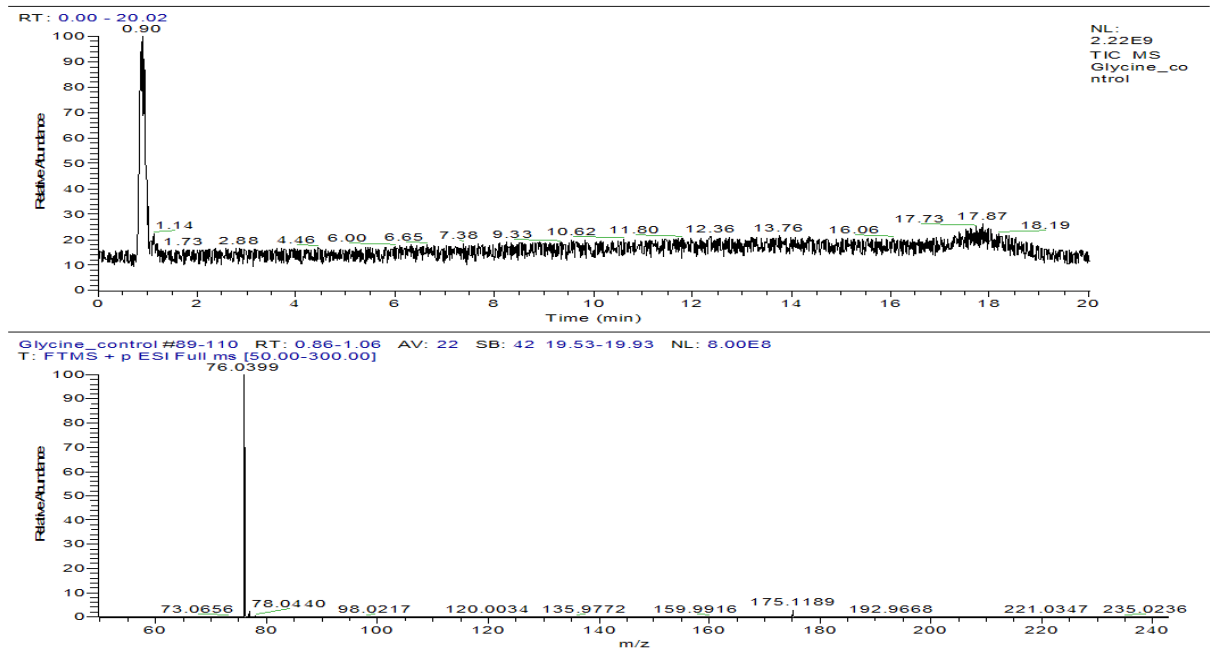


Fig. S14.

Fig. S15.

Fig. S16.

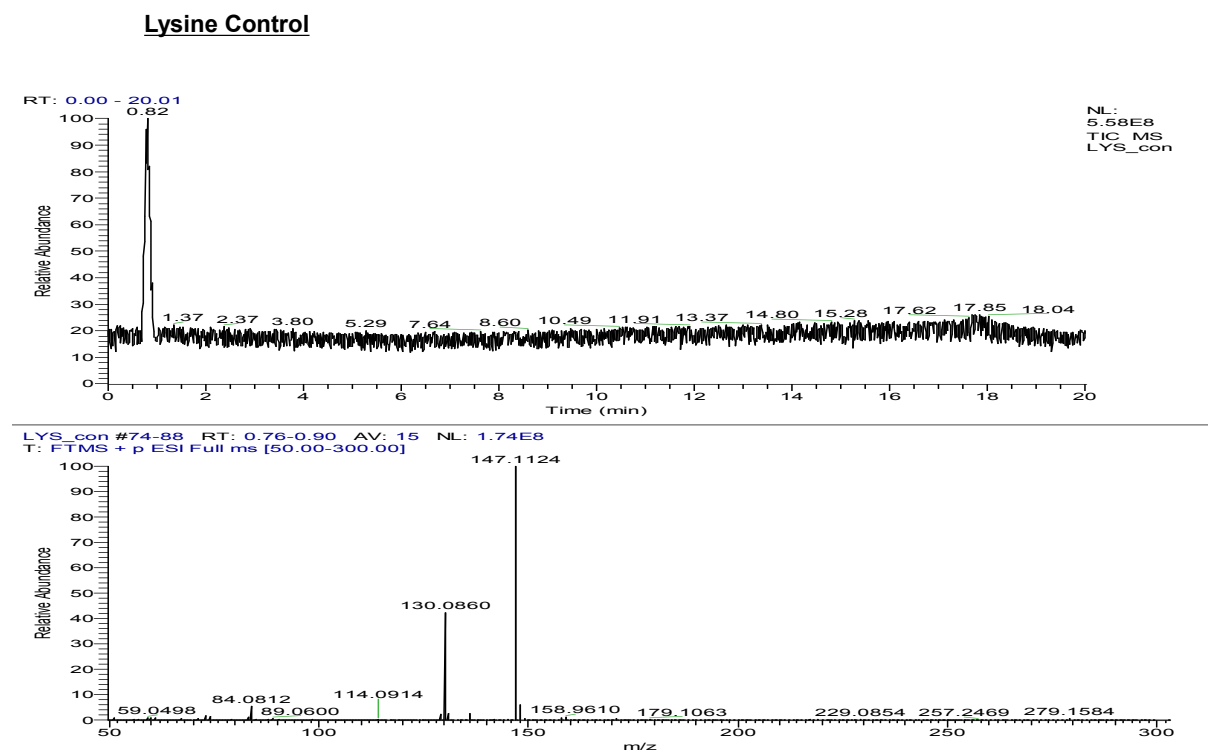


Fig. S17.

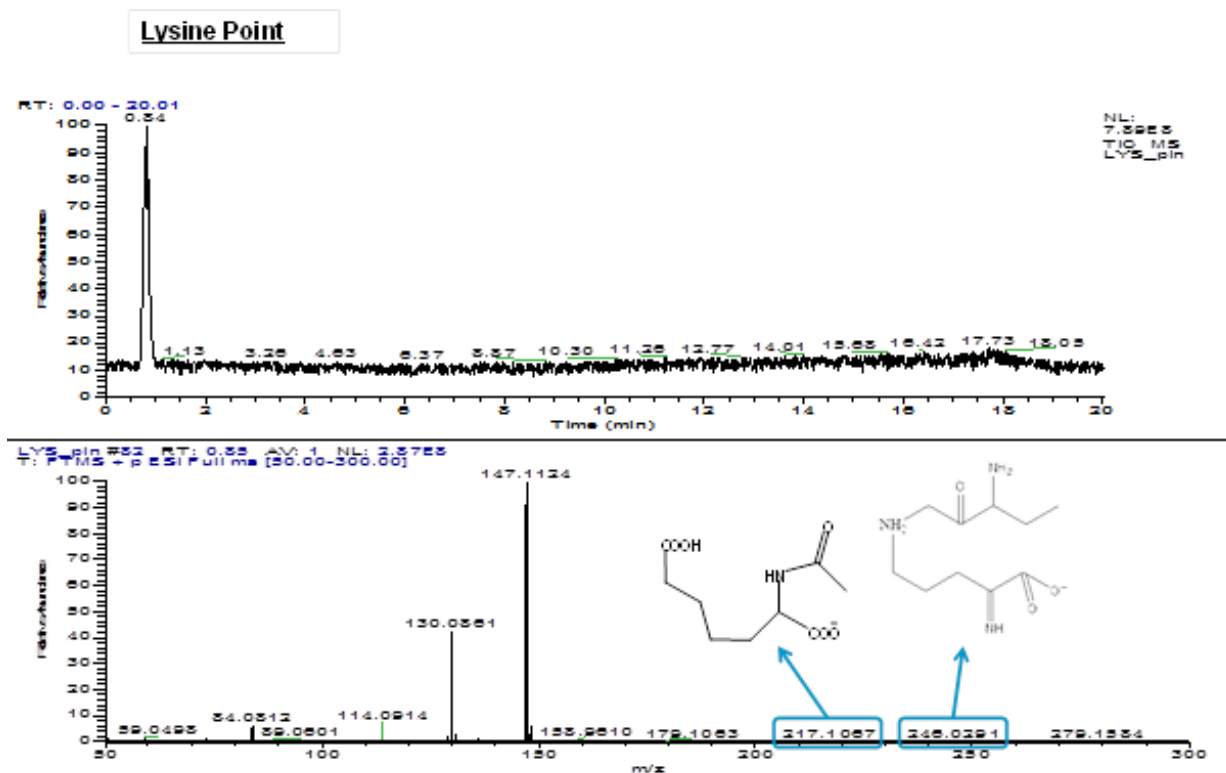


Fig. S18.

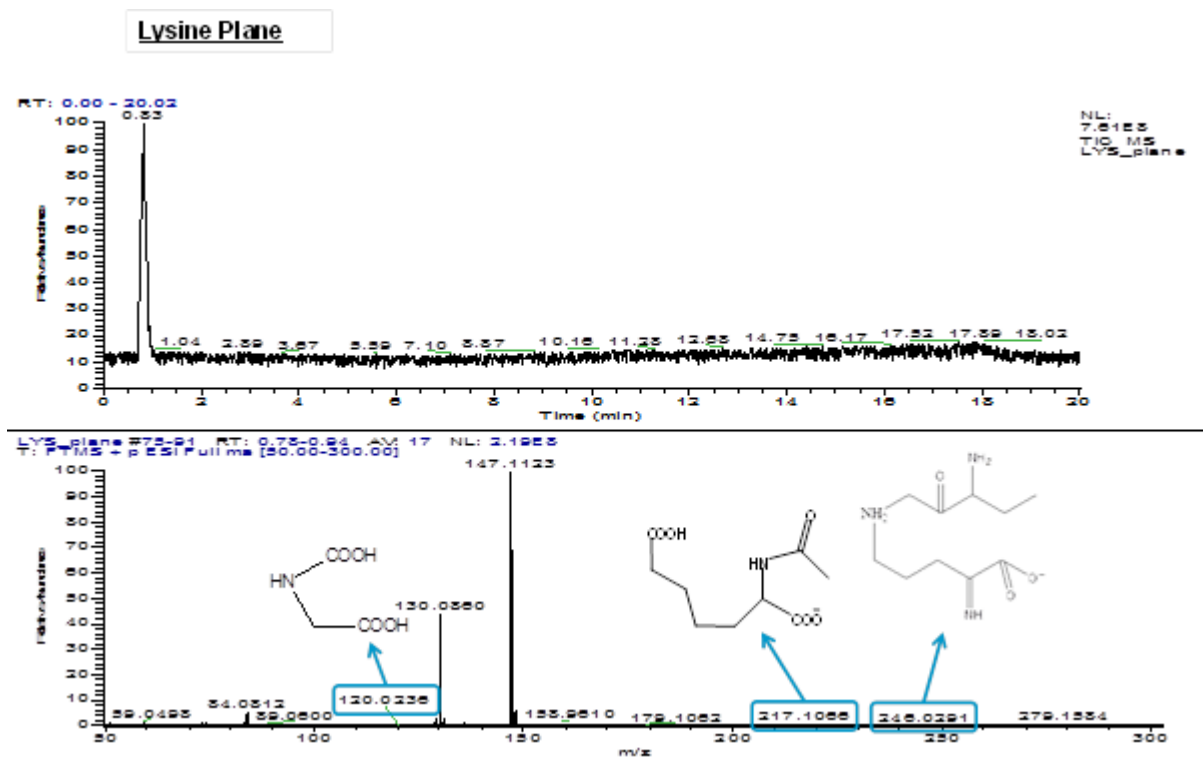


Fig. S19.

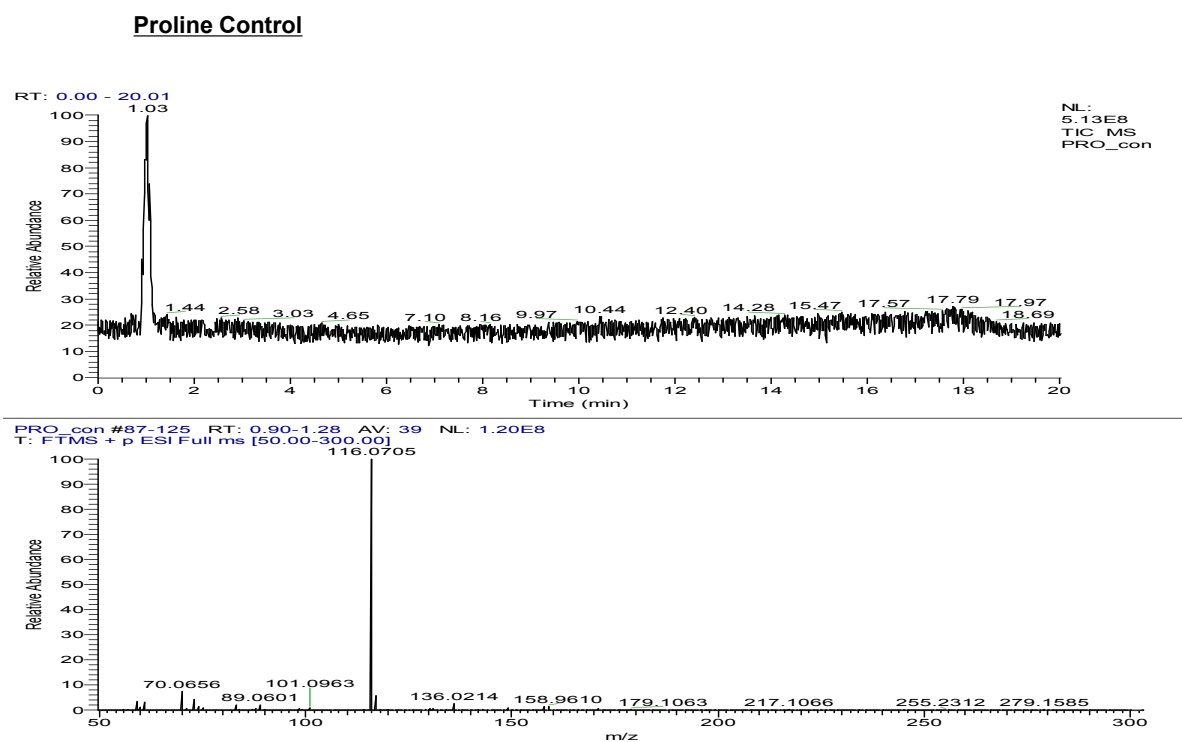


Fig. S20.

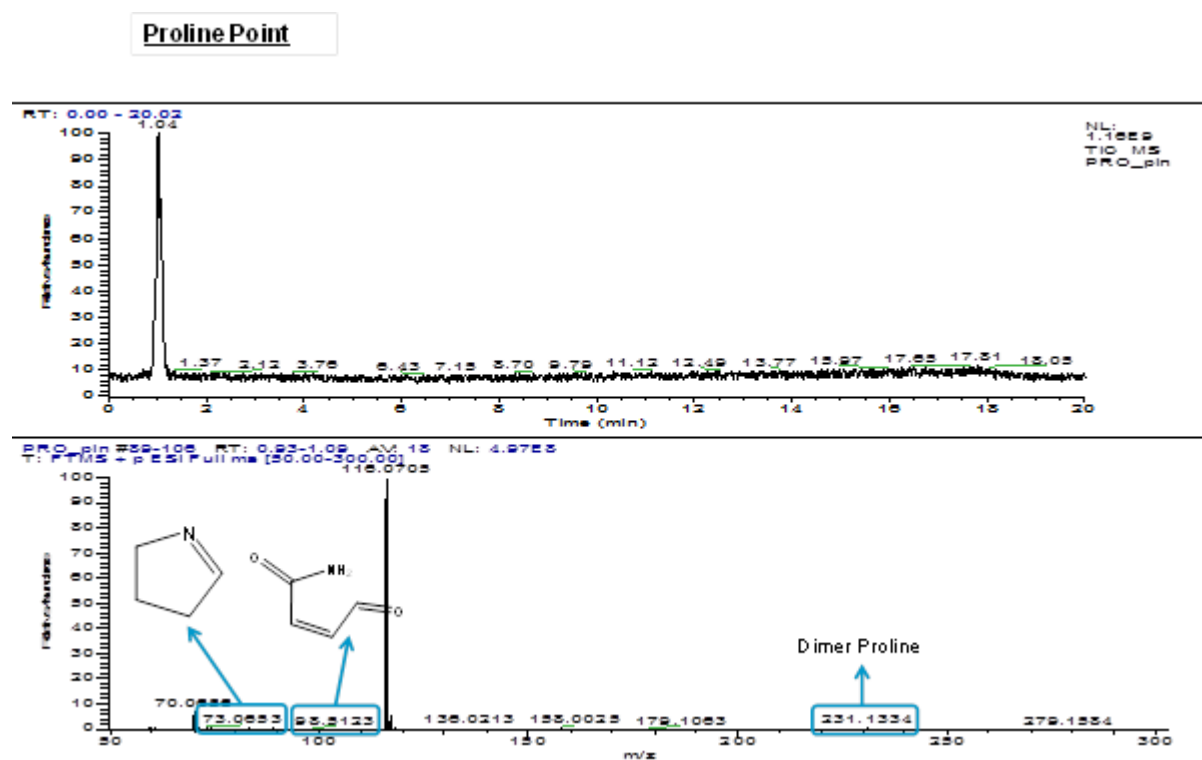


Fig. S21.

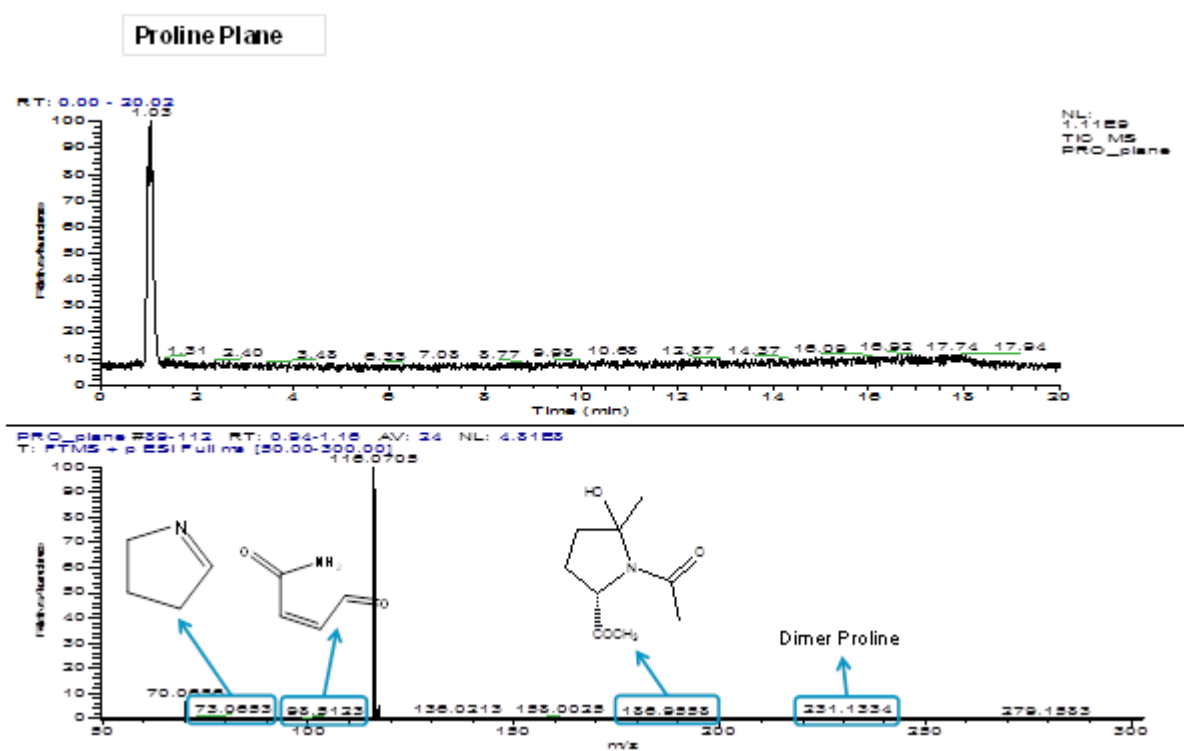


Fig. S22.

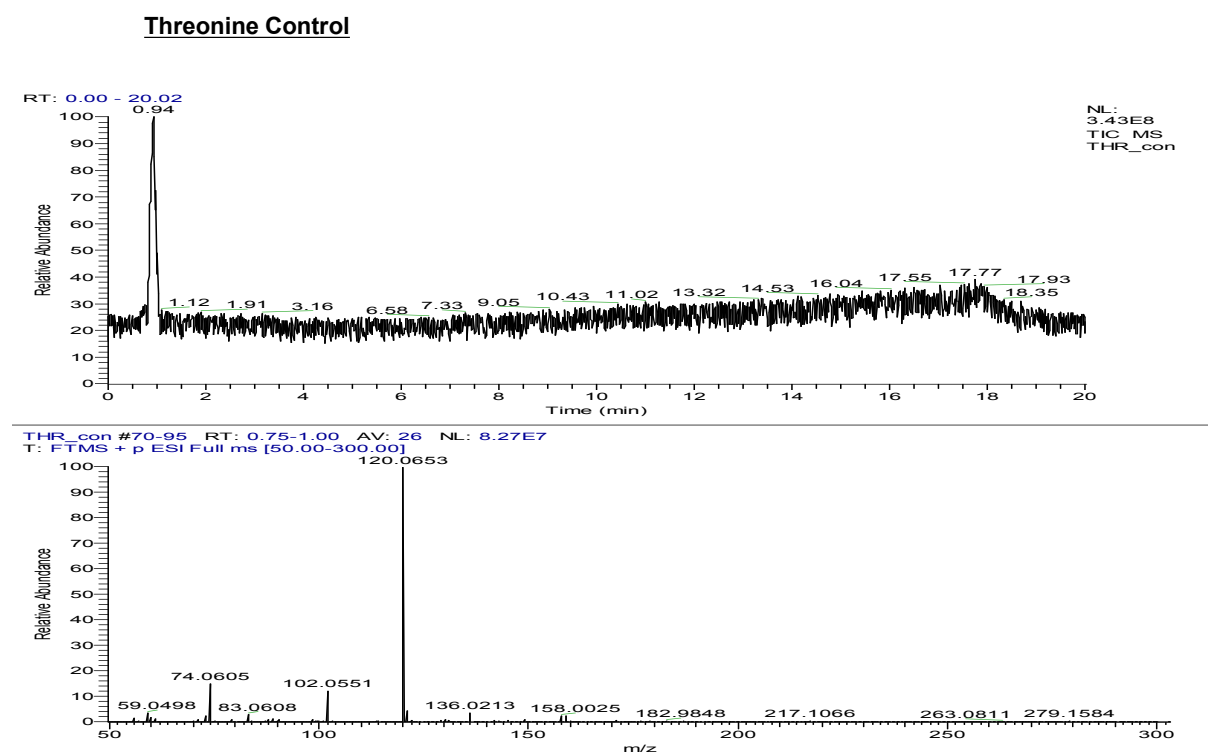


Fig. S23.

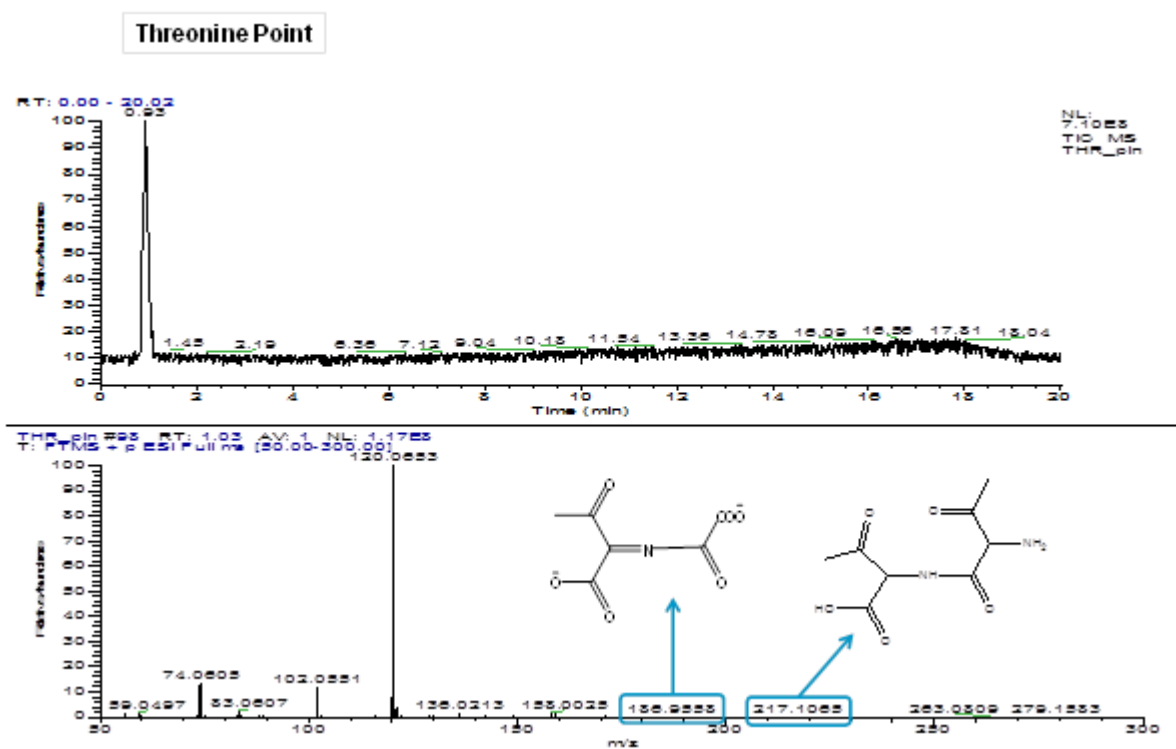


Fig. S24.

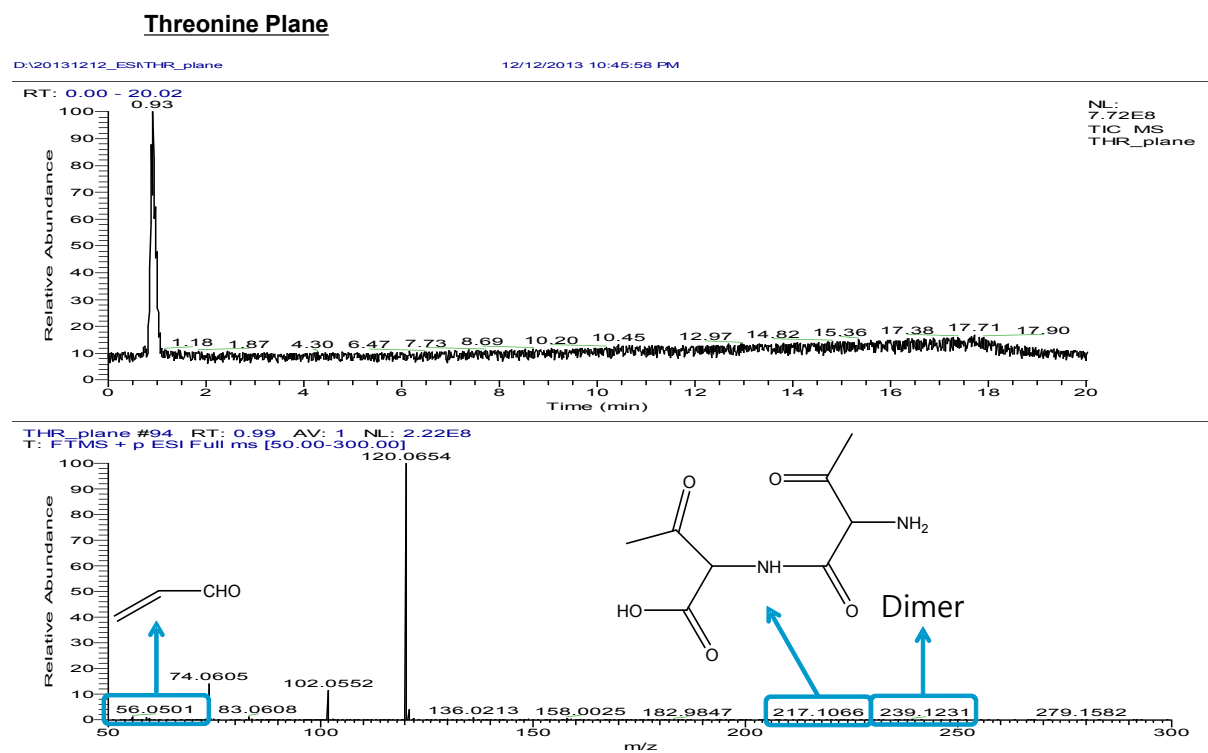


Fig. S25.